Publications

Available Online

J. Sci. Res. **16** (1), 107-114 (2024)

JOURNAL OF SCIENTIFIC RESEARCH

www.banglajol.info/index.php/JSR

Solar Plasma Structures and Solar Wind Plasma Turbulences in Relation with Geomagnetic Disturbances during Decline Phase of Solar Cycle 24 and Rising Phase of Solar Cycle 25

S. Kumar [1•], R. Sharma[1], O. P. Tripathi[1], P. L. Verma[2]

[1]Department of Physics, AKS University, Satna, Madhyapradesh, India

[2]Department of Physics, Government Vivekananda P. G. College Maihar, Satna, Madhyapradesh, India

Received 3 April 2023, accepted in final revised form 13 September 2023

Abstract

We have studied the effect of solar structures and turbulences in solar wind plasma on the Earth's magnetosphere during the decline phase of solar cycle 24 and the rising phase of solar cycle 25. Most CMEs are geoeffective, cause geomagnetic storms, and are associated with C-class and M-class solar flares (S.F.s). It is also observed that these geomagnetic storms are associated with disturbances in solar wind plasma parameters. We have determined a large positive correlation with a correlation coefficient of 0.68, 0.58, 0.65, and 0.63 between the magnitude of the extensive geomagnetic storms and the peak value of IMF B_{total}, the magnitude of IMF B_{total}, the peak value of disturbances in the southward component of interplanetary magnetic fields (IMF Bz), and magnitude of disturbances in the southward component of interplanetary magnetic fields (IMF Bz). The correlation coefficient of 0.61 is higher between the magnitude of Dst and the magnitude of SWPT, as compared with the magnitude of flow pressure (0.39). From the present work, we have concluded that solar plasma structures and solar wind turbulences are mainly responsible for generating extensive geomagnetic storms.

Keywords: Solar plasma parameters; Coronal mass ejections (CMEs); Interplanetary magnetic field (IMF); Geomagnetic storms.

doi: http://dx.doi.org/10.3329/jsr.v16i1.65392 J. Sci. Res. **16** (1), 107-114 (2024)

1. Introduction

The solar wind is a stream of energized charge particles ejected from the Sun's outermost atmosphere, called the corona. It provides a highly variable source of energy to the interplanetary medium. The large-scale evolution of the solar wind is determined by the solar magnetic field, whose structure varies during the solar cycle [1-3]. The solar magnetic field carried outward by the solar wind in the heliosphere when the highly conductive solar wind plasma drives the Sun's magnetic field lines is called the interplanetary magnetic field (IMF) [4]. Solar yield in the form of solar plasma and magnetic field driven out into interplanetary medium subsequently produces disconcertion

[•] *Corresponding author*: saket301190@gmail.com

in the geomagnetic field. When these plasma and fields reach the earth's mesosphere, they produce superfluous ionization in the sunlit part of the earth and display irregular storm time charges in the pragmatic geomagnetic field.

Solar wind plasma continuously streams out of the Sun during interplanetary space at typical speeds of 400–500 km/s, breaking the Sun's magnetic field frozen into it. The dynamics of this wind is responsible for 91.5 % of geomagnetic activity [5-7]. The solar wind and the magnetosphere constantly interact, thus constituting a coupled system, because the disturbances of the interplanetary medium cause geomagnetic disturbances [8]. Superposed on this ambient plasma are transient injections of material, often faster than the solar wind and also carrying a strong magnetic field, known as coronal mass ejections.

According to coronal mass ejections and co-rotating interaction regions/high-velocity fluxes striking the earth's magnetic field are the main drivers of geomagnetic activity [9, 10]. Coronal mass ejections produce the majority of extensive geomagnetic storms, and co-rotating/high-velocity flux interaction regions produce a large proportion of minor to moderate geomagnetic storms. Earth's magnetic field forms the cavity, shielding Earth from a variety of interplanetary structures known as the magnetosphere. The highest solar wind speeds are observed during the descending phase of the solar cycle, when high-velocity flows from equatorward extensions of polar coronal holes often reach low heliographic latitudes and the ecliptic plane [5,11]. If the solar wind magnetic field is such that its direction points anti-parallel to earth's magnetic field, energy can be injected into the magnetosphere, increasing the equatorial ring currents, differential gradient, and curvature drift of electrons and protons in the near earth region, causing geomagnetic storms.

Large geomagnetic storms are usually caused by structures in the solar wind having specific features: long durations of strong southward interplanetary magnetic field (IMF) impinging on the earth's magnetosphere. These features are effective in causing geomagnetic disturbances and are said to be geoeffective. The variation of Earth's magnetic field, usually expressed through magnetograms, shows the time variation of declination (D), vertical component (Z), and horizontal component (H). However, for global quantitative representation, various geomagnetic indices have been introduced. The disturbances storm time (Dst) index is the conventional measure of ring current intensity and energy observed at Earth's surface over low and moderate latitudes.

The Dst values are obtained from the longitudinal average of H variations measured at middle and low-latitude observatories. It is the best indicator of the ring current intensities and a sensitive index representing the degree of solar disturbances. The statistical study presented in this paper aims to analyze the effect of extensive geomagnetic storms and their association with solar wind plasma temperature and IMF during the decline phase of the solar cycle 24 and the rising phase of the solar cycle 25. Today's challenge for Space Weather research is to quantitatively predict the dynamics of the ionosphere and magnetosphere from measured solar wind interplanetary conditions. A number of correlative studies between the extensive geomagnetic storms and the various

interplanetary field and plasma parameters have been performed to search for causes of geomagnetic activity and for developing models for predicting geomagnetic storms [15-19].

2. Data Analysis Methods

In the present study, we have observed 15 geomagnetic storms with (Dst ≤-100 nT) during the period of decline phase of solar 24 and the rising phase of solar cycle 25. If the magnitude of the storm (Dst ≤ -100nT) recurs for several consecutive days/hours, then the last day/hour is taken as the storm's day. Here, we have taken a set of six extensive large geomagnetic storms (Dst ≤-125 nT) and analyzed them with different solar and interplanetary disturbances like IMF B, IMF Bz, and S.W. Parameters (temperature, velocity, and pressure). Solar Geophysical Data (Prompt Comprehensive report) of U.S. Department of Commerce, NOAA and omni web data have obtained the hourly Dst values for geomagnetic storms [12-14]. The coronal mass ejection (CMEs) data have been obtained by SOHO/LASCO CME CATALOG. This CME catalog is generated and maintained at the CDAW Data Center by NASA and The Catholic University of America in cooperation with the Naval Research Laboratory SOHO, which is a project of international cooperation between ESA and NASA. The magnetic cloud and interplanetary shocks database of Helio-spheric Shock Waves has obtained data maintained at the University of Helsinki. The database currently includes the shocks from ACE, Wind STERO, Helios, Ulysses, and Cluster spacecraft.

Table 1. Characteristic features of geomagnetic storms occur during the decline phase of the solar cycle 24 and the rising phase of the solar cycle 25.

Date of event	Maximum Mag. of event, nT	IMF(B_{total}) nT		IMF (Bz) nT		SWPT K		SWPS Km/s		Flow Pressure nPa		Types of CMEs	Types of solar flares
		Maximum	Magnitude	Maximum	Magnitude	Maximum	Magnitude	Maximum	Magnitude	Maximum	Magnitude		
07.01.2015	-107	21.6	15.8	-17.1	-15.9	2E+05	1E+05	508	88	9.86	7.06	PH	M
10.01.2015	-234	31.5	23.7	-24.1	-22.9	8E+05	8E+05	614	202	7.92	5.68	PH	M
14.01.2015	-198	37	27.3	-26.3	-25.1	1E+06	1E+06	742	336	9.53	9.29	H	M
16.08.2015	-100	21.7	12.5	-9.6	-8.2	3E+05	3E+05	540	210	8.42	6.98	PH	C
27.08.2015	-103	14.2	5.8	-13.1	-6.4	2E+05	1E+05	460	124	8.03	5.03	H	M
07.10.2015	-130	20.4	11.1	-8.6	-7	6E+05	6E+05	775	347	9.51	5.6	PH	M
20.12.2015	-166	19.5	11.9	-18.1	-11.2	1E+05	1E+05	428	35	9.13	7.57	H	C
01.01.2016	-102	16.9	11.4	-16.1	-14.6	3E+05	3E+05	477	146	9.92	9.58	H	C
20.01.2016	-101	16.9	11.2	-11.5	-7.8	4E+05	4E+05	547	208	9.47	5.4	H	C
06.03.2016	-102	20.1	14.7	-8.5	-6.7	5E+05	5E+05	590	231	9.85	7.63	PH	B
13.10.2016	-109	24.1	19.9	-19.3	-18.3	3E+05	3E+05	719	237	4.18	2.58	H	B
28.05.2017	-125	22.8	20.7	-21.4	-19.6	1E+05	84920	539	203	5.87	3.94	PH	B
08.09.2017	-122	27.3	19.5	-23.6	-21.7	3E+06	3E+06	817	344	7.93	5.13	H	X

26.08.2018	-175	18.2	12	-14.7	-11.1	3E+05	3E+05	573	196	6.02	4.01	NA	B
04.11.2021	-105	22.3	19.8	-15.5	-13.5	1E+06	1E+06	762	279	9.88	8.15	H	M

3. Results and Discussion

Table 2. Occurrence of geomagnetic storms per year during the decline phase of SC 24 and rising phase of SC 25.

Year	Occurrence of Geomagnetic Storms
2015	7
2016	4
2017	2
2018	1
2021	1

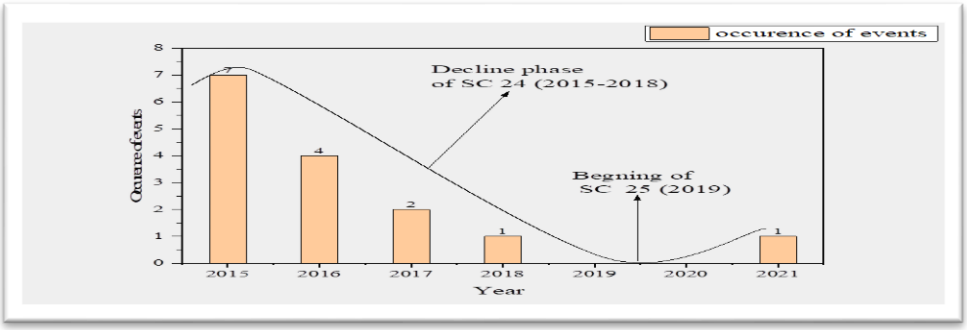

Fig. 1. Frequency histogram of geomagnetic occurrence during the decline phase of SC 24 and rising phase of SC 25.

The characteristic features of all those geomagnetic storms, which are compiled in Table 2, are described here. In this study, we found that 09 (60 %) out of 15 are intense geomagnetic storm events, 05 (33.3 %) out of 15 are major geomagnetic storms, and only 01 out of 15 events are severe geomagnetic storms. Generally, it is believed that the majority of major geomagnetic storms occur during the maximum phase of the sunspot cycle because many solar active regions appear during this time, while a few of the geomagnetic storms are observed during the minimum phase of the sunspot cycle due to the presence of coronal holes and some other solar activities.

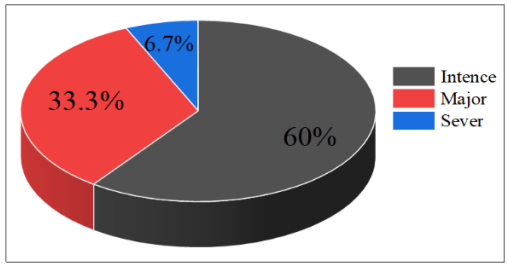

Fig. 2. Different types of geomagnetic storms that occurred during the decline phase of SC 24 and SC 24.

3.1. *Geomagnetic storms and CMEs*

The data analysis of geomagnetic storms associated with coronal mass ejections observed during the period of decline phase of SC 24 and the rising phase of SC 25**,** it is observed that all extensive geomagnetic storms are associated with halo and partial halo coronal mass ejections (CMEs). The association rates of partial halo and halo coronal mass ejections are 67 % and 33 %, respectively. It is also determined that most of the associated CMEs are of higher speed CMEs.

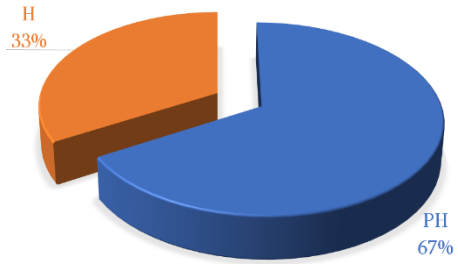

Fig. 3. The percentage of different kinds of associated CMEs.

3.2. *Geomagnetic storms and x-ray solar flares (S.F.s) of different kinds*

The data analysis of extensive geomagnetic storms, associated with Hard X-Ray solar flares of different kinds it is observed that all the extensive geomagnetic storms are Hard X-Ray solar flares of different categories. The association rates M-Class, C-Class, and B-Class X-ray solar flare are M-Class-50 %, C-Class -17 %, and B-Class -33 %, respectively.

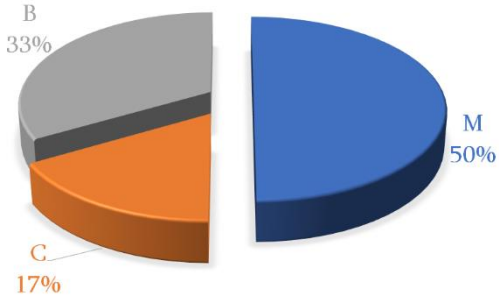

Fig. 4. The percentage of different classes of solar flares.

3.3. *Geomagnetic storms and radio burst*

The data analysis of geomagnetic storms associated with radio bursts of different types during the investigation. The association rate of Type-II and Type IV radio bursts is given below: Type II- 51.60 % and Type IV-48.40 %.

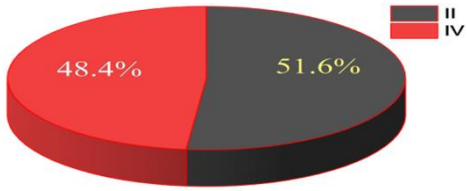

Fig. 5. Different types of radio bursts.

3.4. *Correlation graphs*

Using statistical analysis, we have observed that all the geomagnetic storms are associated with irregularities in solar parameters. We have determined a large positive correlation with a correlation coefficient of (0.68) between the magnitude of the extensive geomagnetic storms and the peak value of disturbances in IMF B_{total}, (0.58) between the magnitude of the extensive geomagnetic storms and magnitude of disturbances in IMF B_{total} (0.65) between the magnitude of the extensive geomagnetic storms and the peak value of disturbances in southward component of interplanetary magnetic fields (IMF Bz), (0.63) between the magnitude of the extensive geomagnetic storms and magnitude of disturbances in southward component of interplanetary magnetic fields (IMF Bz). The correlation between the magnitude of Dst and the magnitude of solar wind temperature (with a positive correlation coefficient of 0.61) is higher than the magnitude of Dst and the magnitude of flow pressure (0.39).

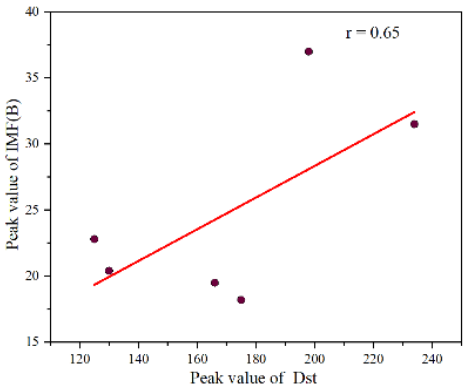

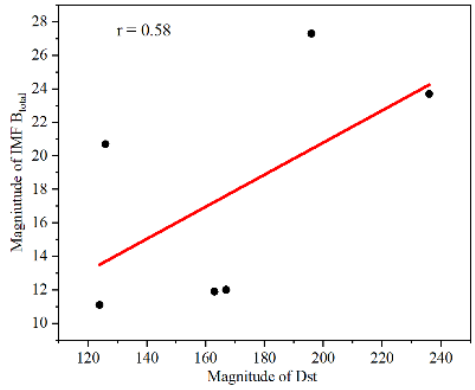

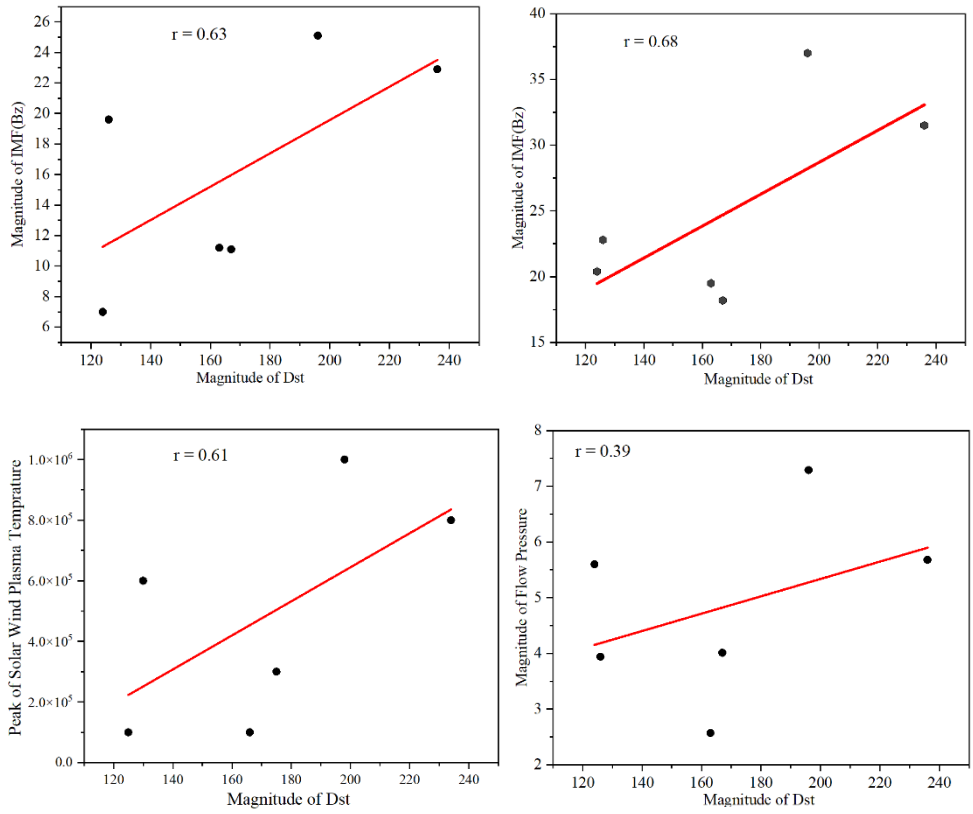

Fig. 6. The scatter plot between peak value of Dst and peak value of IMF (B) in upper left panel, magnitude of Dst and magnitude of B_{total} in upper right panel, magnitude of Dst and peak value of B_z in middle left panel, magnitude of Dst and magnitude of B_z in middle right panel, magnitude of Dst and peak value of solar wind plasma temperature in lower left panel, and magnitude of Dst and magnitude of flow pressure in lower right panel.

4. Conclusion

It has been verified that extensive geomagnetic storm intensity is correlated well with the interplanetary magnetic field IMF (B_{total} and B_z) better than with its solar parameters (SWPT and Flow Pressure). (b) Magnitude of Dst and Magnitude of B_{total}

Type II- 51.60 % and Type IV-48.40 % are responsible for occurrence of geomagnetic storms.

M-Class-50 %, C-Class -17 % and B-Class -33 % solar flares of different kinds are responsible for occurrence of geomagnetic storms.

67 % partial halo and 33 % halo CMEs are identified during the occurrence of geomagnetic storms in this study.

It is believed that the majority of extensive geomagnetic storms occur during the maximum phase of sunspot cycle, because many solar active regions appear during this time, while a few of the geomagnetic storms are observed during the minimum phase of sunspot cycle due to the presence of coronal holes and some other solar activities.

Acknowledgment

In this investigation data has been taken from the NSSDC Omni web data system which is obtained from online. So, author thanks for providing data online which is supporting in future research. The author thanks the Omni web Explorer for providing these satellite data.

References

1. Y. M. Wang, N. R. Jr. Sheeley, and A. G. Nash, Astrophys. J. **383**, 431 (1991). https://doi.org/10.1086/186235
2. P. L. Verma, S. Kumar, D. Ochani, V. Pandey, and A. Shukla, Eur. Acad. Res. **8:11**, 6948 (2021).
3. R. F. Pinto, A. S. Brun, L. Jouve, and R. Grappin, Astrophys. J. **737:72**, 1 (2011). https://doi.org/10.1088/0004-637X/737/2/72
4. E. N. Parker, Astrophys. J. **128**, 664 (1958). https://doi.org/10.1086/146579
5. J. P. Legrand, M. Le Goff, and C. Amory-Mazaudier, Annales Geophys. **8**, 637 (1990).
6. J. L. Zerbo, C. Amory-Mazaudier, O. Frédéric, and J. D. Richardson, Annales Geophysicae, **30**, 421 (2012). https://doi.org/10.5194/angeo-30-421-2012
7. R. D'Amicis, D. Telloni, and R. Bruno, Frontiers Phys. **8**, 4857 (2020). https://doi.org/10.3389/fphy.2020.604857
8. I. G. Richardson, D. F. Webb, J. Zhang, D. B. Berdichevsky, D. A. Biesecker, et al., J. Geophys. Res.: Space Phys. **111**, A07S09 (2006). https://doi.org/10.1016/j.asr.2005.06.049
9. J. Zhang, I. G. Richardson, D. F. Webb, N. Gopalswamy, E. Huttunen et al., J. Geophys. Res.: Space Phys. **112**, A10102 (2007). https://doi.org/10.1016/j.asr.2006.05.027
10. J. T. Gosling, J. R. Asbridge, S. J. Bame, and W. C. Feldman, J. Geophys. Res. **81**, 5061 (1976). https://doi.org/10.1029/JA081i013p02111
11. K. Hakamada, and S. I. Akasofu, J. Geophys. Res.: Space Phys. **86**, 1290 (1981). https://doi.org/10.1029/JA086iA03p01290
12. S. Kumar, O. P. Tripathi, R. Sharma, and P. L. Verma, Int. Astron. Astrophys. Res. J. **5**, 65 (2023).
13. O. P. Tripathi and P. L. Verma, IJSR **2**, 412 (2013).
14. O. P. Tripathi and P. L. Verma, IJAR **3**, 50 (2013).
15. E. Echer, M. V. Alves, and W. D. Gonzalez, Solar Phys. **221**, 361 (2004). https://doi.org/10.1023/B:SOLA.0000035045.65224.f3
16. W. D. Gonzalez and B. T. Tsurutani, Planet. Space Sci. **38**, 181 (1987). https://doi.org/10.1016/0032-0633(90)90082-2
17. N. Gopalswamy, S. Akiyama, S. Yashiro, G. Michalek, and R. P. Lepping, J. Atmos. Solar-Terrestrial Phys. **70**, 245 (2008). https://doi.org/10.1016/j.jastp.2008.06.010
18. B. S. Rathore, S. C. Kaushik, R. M. Bhadoria, K. K. Parashar, and D. C. Gupta, Indian J. Phys. **86**, 563 (2012). https://doi.org/10.1007/s12648-012-0106-2
19. B. S. Rathore, D. C. Gupta, and K. K. Parashar, Int. J. Geosci. **5**, 1602 (2014). https://doi.org/10.4236/ijg.2014.513131